catalysts

MDPI

Article

Congo Red Dye Degradation by Graphene Nanoplatelets/Doped Bismuth Ferrite Nanoparticle Hybrid Catalysts under Dark and Light Conditions

Sabeen Fatima [1,†], S. Irfan Ali [2,†], Muhammad Z. Iqbal [3,*] and Syed Rizwan [1,*]

1 Physics Characterization and Simulations Lab (PCSL), School of Natural Sciences (SNS), National University of Sciences and Technology (NUST), Islamabad 44000, Pakistan; khushi.khar@gmail.com
2 Shenzhen Key Laboratory of Advanced Thin Films and Applications, College of Physics and Energy, and Key Laboratory of Optoelectronic Devices and Systems of Ministry of Education and Guangdong Province, College of Optoelectronic Engineering, Shenzhen University, Shenzhen 518060, China; irfansyed715@gmail.com
3 Department of Chemical and Petroleum Engineering, United Arab Emirates University (UAEU), Al-Ain 15551, United Arab Emirates
* Correspondence: mziqbal@uaeu.ac.ae (M.Z.I.); syedrizwan@sns.nust.edu.pk or syedrizwanh83@gmail.com (S.R.); Tel.: +97137135398 (M.Z.I.); +9290855599 (S.R.)
† Sabeen Fatima and S. Irfan Ali are equal contributors.

Received: 22 February 2020; Accepted: 23 March 2020; Published: 30 March 2020

Abstract: The continuously growing need for clean water has increased research looking for new and efficient ways to treat wastewater. Due to its magnetic properties, Bismuth ferrite, a photo-catalyst, has introduced a novel field of photo-catalysis where the photo-catalytic material could easily be separated from the aqueous solution after wastewater treatment. Herein, a new type of photo-catalysts, composed of Gadolinium (Gd) and Tin (Sn), co-doped Bismuth Ferrite deposited over graphene nanoplatelet surface have been synthesized using a two-step method. In first step, Gd (fixed concentration 10%) and Sn (5%, 15%, 20% and 25%) were doped inside bismuth ferrite (BFO) host using sol-gel method (namely the BGFSO nanoparticles, abbreviated for Gd and Sn doped BFO). In the second step, BGFSO nanoparticles were introduced onto GNPs using co-precipitation method (namely the BGFSO/GNP nanohybrids). The x-ray photoelectron spectroscopy confirmed the chemical bonding between co-doped BFO and GNP sheets via oxy and hydroxyl groups. The photocatalytic activities of the nanohybrids under both, visible light and dark conditions have been increased, and the maximum degradation activity (74%) of organic dye Congo-red (CR) is obtained for 25% Sn-doped BGFSO/GNP nanohybrid. The photocatalytic activity may be attributed to enhanced adsorption capability, electron storage properties of graphene and the presence of oxygen-rich species inside nanohybrids. Based on the current overgrowing population and need for clean water, these materials present versatile potential as catalysts for wastewater treatment.

Keywords: Sn and Gd co-doped BFO; graphene platelets; nanohybrids; photocatalytic activity; visible light; dark conditions

1. Introduction

Photocatalysis deals with the occurrence of oxidation and reduction reactions on the surface of a solid material (photo-catalyst) due to photogenerated charge carriers (holes and electrons) [1]. For the last two decades water contamination has increased, due to over industrialization, requiring materials to treat waste water more efficiently [2]. Large organic matter (waste), which is difficult to adsorb, can be broken into smaller nonhazardous molecules using photocatalysis. Semiconductor oxides are

emerging as promising and efficient photo-catalysts under UV-light irradiation [1,3–5]. Among earlier photocatalysts, titanium oxide (TiO_2) has been widely researched photo-catalytic material with a short coming of a wide band-gap which renders it to utilize the complete solar spectrum effectively [6].

Perovskite structures have gained great attention, due to their fascinating physical characteristics, and initiated many useful applications in different technological areas [7–9]. Perovskites are materials having chemical formula ABO_3 [10] where, A is usually a bigger cation than B cation and O is oxygen (anionic specie). The key features of perovskite materials include simple and easy fabrication, huge solar adsorption, less non-radiative charge carrier recombination, high mobility of carriers for cell architectures and capitalization of dye sensitized photovoltaic cells [9]. Among perovskites, bismuth ferrite $BiFeO_3$ (also denoted as BFO) has been enormously attractive due to its multiferroic properties. BFO belong to the class of rhombohedral perovskites with space group named R3c and possesses ferroelectric and ferromagnetic properties simultaneously [11–15]. BFO is considered to be among the highly efficient visible light-driven photocatalysts [16–18]. Upon visible light irradiation, electrons move towards conduction bands, creating holes in the valance band, leading to degradation of organic pollutants by oxidation and reduction reactions [15]. The band-gap in perovskites can be tuned by various methods for catalytic applications. Specifically, the band-gap in BFO can be tuned by doping with rare-earth or transition metals [19–23], fabricating its hybrid or composite structures with other materials such as graphene [24–27]. Co-substitution of bismuth and iron inside bismuth ferrite has been reported many times with enhanced electric, magnetic and photocatalytic properties [28–30]. Based on published reports, rare-earth metal doping, inside BFO, improved its physical and chemical properties drastically [16–19,23,31]. The doping of Sn on B site of BFO has shown a good tuned structure for catalytic and sensing applications [10]. The substitution of Gd on the A site of BFO has shown enhanced ferromagnetism and visible light catalytic effects with improved surface chemistry [21,22]. A few reports have also been published on the doping of Gadolinium (Gd) and Tin (Sn), showing enhanced photocatalytic properties of the prepared co-doped nanoparticles and hybrid systems [17,23,31]. The substitution of Gd and Sn inside BFO transforms the lattice structure from rhombohedral to distorted rhombohedral, and then to orthorhombic due to unit cell expansion, as a result of the ionic radii difference among Bi^{3+} (1.03 Å), Gd^{3+} (0.938 Å), Sn^{4+} (1.09 Å) and Fe^{3+} (0.78 Å) [17,23,31]. The addition of Sn and Gd inside BFO also tuned the band-gap of the system, which in turns, assists in fast electron-hole pair generation for higher photocatalytic activity.

Graphene is a two-dimensional (2D) allotropic form of carbon with remarkable properties, such as excellent electrical conductivity, splendid absorptivity, large surface area and thermal and chemical stability [32–36]. Graphene has shown good potential for environmental applications [19,21,32,37]. Graphene, in combination with BFO, acts as an e-trapping medium that enables effective separation of electron-hole charge carriers and lowers the recombination rate accompanied by an increase in photocatalytic activity [38]. As the pristine graphene is very costly and difficult to synthesize, recently a cost-effective multilayer graphene product [39], named graphene nanoplatelets (GNP), is emerging as a good candidate for many applications, such as dye sensitized solar cells [40], supercapacitors [41], etc. GNP hybrids with MgO has be used, and has shown good photocatalytic activity in the degradation of organic dye methyl orange [42]. On the other hand, graphene hybrids with BFO and co-doped BFO has shown a good catalytic behavior with high surface area, more active sites for carriers and low band-gap [14,16,31]. All these properties play a key role in the removal of organic contaminants.

Herein, Gadolinium (Gd) and Tin (Sn) co-doped bismuth ferrite (BFO) nanoparticles (BGFSO) were synthesized using sol-gel method. Graphene nanoplatelets (GNPs) were combined with the BGFSO nano-particles to form hybrids and used for photocatalytic application. BGFSO-GNP hybrid have shown good catalytic degradation under visible light, as well as dark, which is proven to be an efficient catalyst, magnetic and can perform catalytic activity without the presence of light (UV or solar light) [43,44].

2. Characterization Details

X-ray diffraction (XRD) was performed using Rigaku-2500 machine (Tokyo, Japan) having Cu-K radiation and the scanning rate was 1°/s within 2θ range from 20° to 60°. A JEOL-7001 Field emission scanning electron microscope (FESEM) (Tokyo, Japan) was used for obtaining the micro images of hybrid structures (sputter coated with platinum). The accelerated voltages in FESEM were kept from 1.5 to 3 keV. The Thermo Scientific Kα x-ray photoelectron spectrometer (Escalab-250) (Massachusetts, U.S) was used for analyzing chemical composition with binding energies. A Hitachi UV-3310 spectrophotometer (Tokyo, Japan) was used for measuring the diffused reflectance spectra (DRS) of BGFSO-GNP nanohybrids. Further for photocatalysis initially Congo red (CR) dye was dissolved in deionized water at a concentration of 100 mg per liter. The photocatalyst (100 mg) was dispersed in dye solution (100 mL) using constant stirring for 2 h under dark conditions. The stirring was performed in an ice bath to avoiding the thermal degradation of organic dye. A Xenon lamp having power of 300W with a cut-off filter of 420 nm wavelength was used as visible light source. A small amount of solution (~3 mL) was removed from the reaction flask periodically with an interval of 30 min, followed by centrifugation at 7000 RPM. The supernatant, collected after centrifugation process, was tested using UV-vis spectrophotometer for the CR concentration.

3. Results

Figure 1 shows the XRD results of GNPs, BGFSO nnaoparticles and BGFSO-GNP nanohybrids. In Figure 1a, the peak at 26.4^{o} represents the (002) plane in pristine graphite, corresponding to the JCPDS card no. 01-0646. However, the intensity and the sharpness of the peak is low and peak broadening indicates increased inter planar spacing and sharpness of the peak has been reduced and inter planar spacing (d) has been increased up to 3.37Å. The particle size was calculated using Scherrer's formula ($D = K\lambda/\beta \cos\theta$) of x-ray diffraction analysis [17,23] and for GNP the particle size is 35 nm which shows a stack of 24 graphene sheets approximately. The pristine graphene is a single layer, but the GNPs synthesized here are indeed agglomerated clusters, composed of multilayered graphene with in a single platelet. The presence of peak (002) inside GNPs is because of bulk fragmentation of the graphite during thermal exfoliation [45,46]. The same plane (002) will also be observed inside the synthesized nanohybrids, which will correspond to GNPs loading inside the ferrite nanoparticles.

Figure 1b shows the XRD traces of Gd and Sn doped BFO, with a varying concentration of Sn from 5%-25%, and a fixed Gd concentration of 10%. All the peaks present in BFO are present in the doped samples with two impurity peaks of Bi_2O_3 and $Bi_2Fe_4O_9$ corresponding to the JCPDS card no. 20-0169. The addition of Gd distort the crystallinity of BFO structure by reducing the peak intensities. The peak intensity of impurity phase Bi_2O_3 is increased with the increasing concentration of Sn. The addition of Sn causes the unit cell expansion due to having bigger ionic radii (1.09 Å), as compared to Fe (0.78 Å), which further changes the rhombohedral structure of BFO into orthorhombic structure and a complete structural transformation is observed by overlapping (104) and (110) peaks [17,23]. A negative peak shift is observed inside the BGFSO nanoparticles (containing Sn concentration from 15% to 25%) attributed to an increase in lattice parameter which occurs due to change in bond length as a result of tensile stress produced inside crystal lattice [17]. In addition, the BFO particle size was reduced from 46 nm to 21.5 for BGFSO-5, 21.6 for BGFSO-15, 23 nm for BGFSO-20 and 23.5 nm for BGFSO-25 because of doping. The XRD patterns for co-doped BFO have also been observed and previously published with similar kinds of planes and peaks [23,31].

In Figure 1c the XRD peaks of all the BGFSO-GNP nanohybrids have been shown. A distinct sharp peak of carbon plane (002) is observed in nanohybrid structures corresponding to GNP, proving that nanohybrids contain both BGFSO particles and GNP sheets. The periodicity of perovskite lattice structure has been suppressed and peaks intensity is reduced due to the presence of GNPs inside the nanohybrids [14,16]. The peaks broadening is attributed to decreased crystallite size of nanohybrids [14]. The impurity phase Bi_2O_3 has been completely vanished during hybrid synthesis while a minority phase $Bi_2Fe_4O_9$ is still present. A negative peak shift is also present inside the

BGFSO-5/GNP, BGFSO-15/GNP and BGFSO/GNP-20 nanohybrids, which indicates that the inter-planar distance of the samples is enhanced. The particle size of nanohybrids is further increased as compared to the BGFSO nanoparticles. The calculated particle size is 20 nm for BGFSO-5/GNP, 19 nm for BGSO-15/GNP, 21.5 nm for BGFSO-20/GNP and 20 nm for BGFSO-25/GNP.

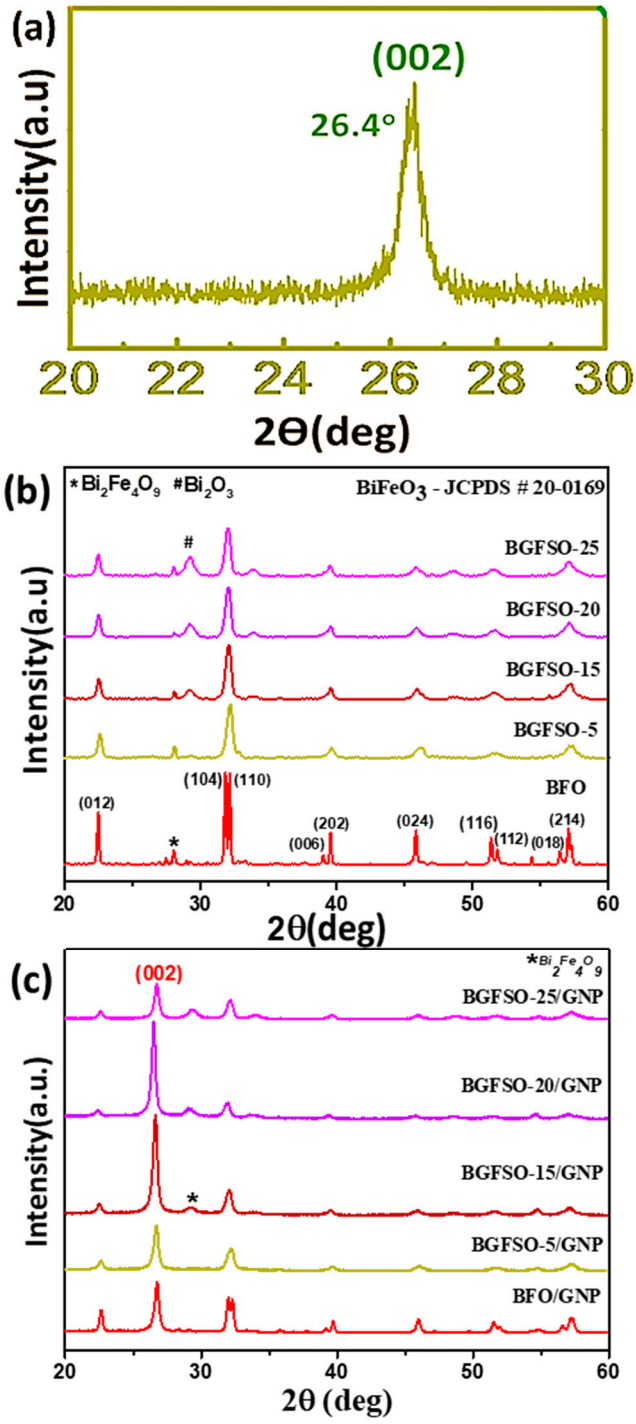

Figure 1. XRD patterns of: (**a**) GNP; (**b**) BGFSO nanoparticles; (**c**) BGFSO/GNP nanohybrids.

3.1. SEM Analysis

Figure 2 shows the morphological analysis of the resulted samples. Transmission electron microscopy (TEM) image of GNPs is shown containing smooth flat graphene sheets with sharp edges with lateral sheet size of around 2-3 microns and the width is 2 microns. In Figure 2b the SEM pattern

of BFO/GNP nanohybrid is shown in which the darker sheet like part is representing GNPs and the lighter granular part is referring to BFO nanoparticles.

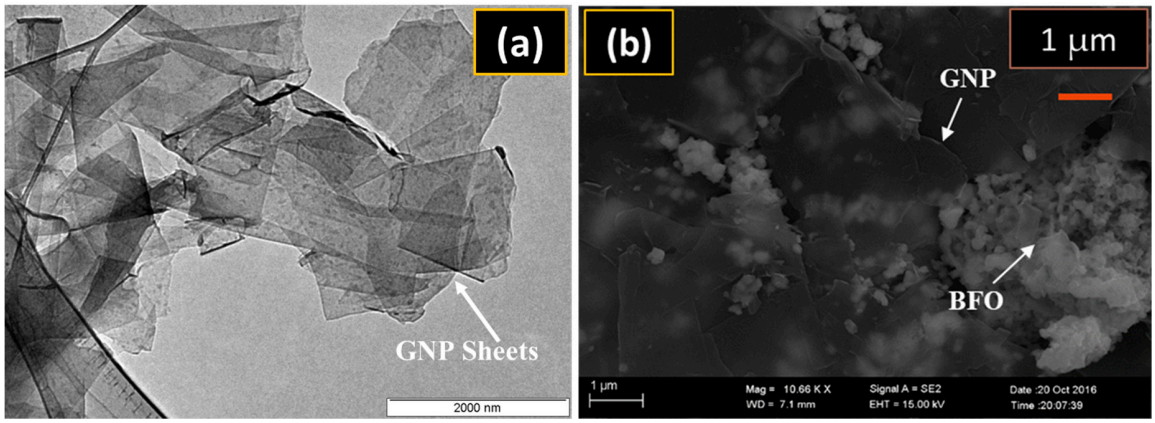

Figure 2. (**a**) TEM results of GNPs, and (**b**) SEM of BFO/GNP hybrid structure.

Figure 3 shows SEM images of all the nanohybrids with varied Sn concentration. As we moved from Figure 3a–d the concentration of Sn varied from 5% to 25%. The SEM confirms the presence of both BGFSO and GNP phases proving the nanohybrid fabrication. The BGFSO nanoparticles are homogeneously distributed over graphene surface at lower Sn concentration (Figure 3a). On the other hand, as the concentration of Sn is increased, an agglomeration of nanoparticles is observed. A large cluster of nanoparticles containing 25% Sn is observed in Figure 3d. The distribution of granular particles due to an ice like transparent effect can be observed over and under the graphene layers. In conclusion, the co-precipitation method helps BGFSO nanoparticles to completely diffuse inside, and over, the graphene sheets.

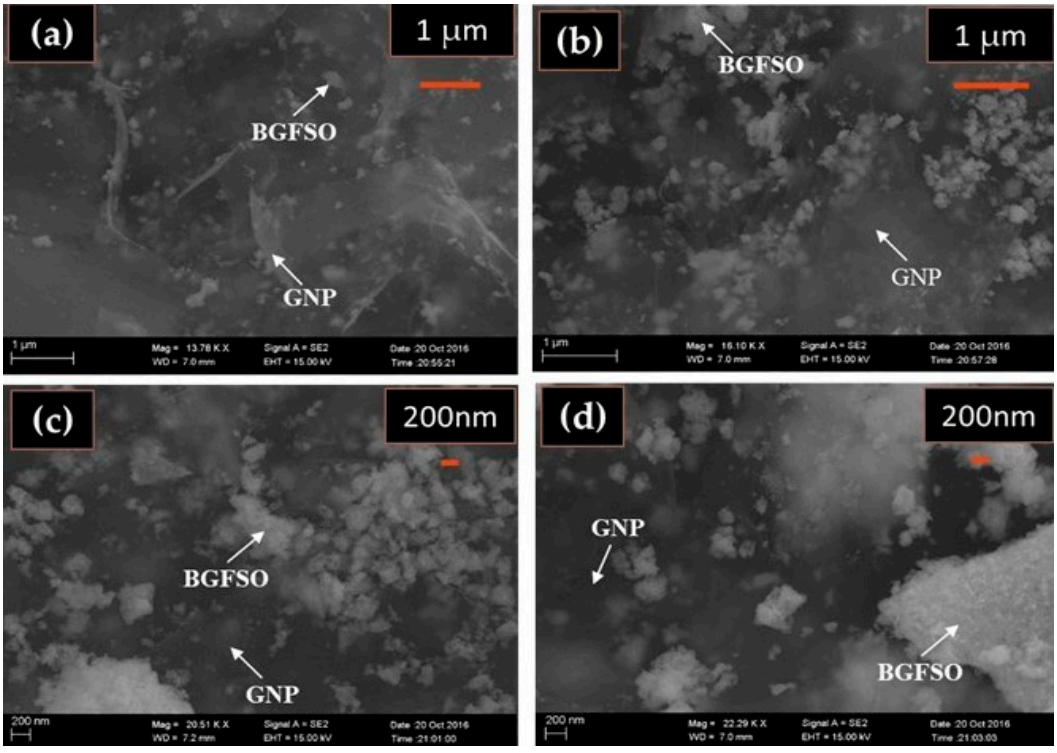

Figure 3. SEM patterns of BGFSO/GNP nanohybrids: (**a**) BGFSO-5/GNP; (**b**) BGFSO-15/GNP; (**c**) BGFSO-20/GNP; (**d**) BGFSO-25/GNP.

3.2. X-ray Photoelectron Spectroscopy (Elemental Analysis)

Figure 4 represents the X-ray Photoelectron Spectroscopy (XPS) spectra of BGFSO/GNP nanohybrids which helps in analyzing the elemental composition of hybrid structures. The main peaks of the spectra representing bismuth (Bi), iron (Fe), gadolinium (Gd), tin (Sn), oxygen (O) and carbon (C), at different corresponding binding energies, are the clear proof of successful synthesis of BGFSO/GNP nanohybrids [47,48]. Further the deconvolution of XPS is shown in Figure 4b–g. In Figure 4b two peaks representing Bi4f are available at 159.1 eV and 164.2 eV while 2 peaks of Bi4d are available at 443 eV and 463 eV [16]. In Figure 4c three peaks of C1s are shown at binding energies corresponding to 284.8 eV, 285.9 eV and 288.7 eV. The first peak at 284.8 eV is representing the C=C (sp2) network of graphene sheets present inside GNPs while the peak at 285.9 eV is for C-C network (possibly can be of carbon tape) and the third peak at 288.7 is for O-C=O network [16,49]. Oxygen spectra in Figure 4d exhibits two peaks of O1s among which one high intensity oxygen peak is at 529.9 eV representing the oxygen atoms of BFO lattice inside the BGFSO/GNP nanohybrids [14,44] while the other is at 531.2 eV which is actually a shift in oxygen peak due to the bonding between carbon network of graphene sheets and BFO via oxy or hydroxyl group [44]. XPS spectra of each Sn and Gd can be seen in Figure 4e,f. Each of two elements have 2 separate peaks, corresponding to the core shell levels of Sn3d and Gd4d. The Figure 4g shows three peaks of iron present in BGFSO network with core shell level Fe2p. The Fe^{+2} spectrum is broad covering the range of 704 eV to 740 eV, and the peak present at 711 eV corresponds to $2p_{3/2}$, while at 730.5 eV corresponds to $2p_{1/2}$. Iron Fe^{+2} presence inside the BGFSO/GNP nanohybrids enhances the adsorption of organic dye over the surface of the catalyst by means of creating more oxygen vacancies [44]. There is peak of OKLL at 976 eV which corresponds to both, GNP and BFO as oxygen vacancies are produced inside BFO during charge compensation and inside the graphene during reduction. All elemental peaks of BGFSO nanoparticles along with the main peaks of pristine GNP [50] exist inside the nanohybrids and the shifting of some peaks (oxygen and carbon) also represent the chemical bonding in between both BGFSO nanoparticles and GNP sheets. There is no additional peak of other functional groups like C-H, COOR and C-O present inside BGFSO/GNP nanohybrid as they are eliminated during the reduction process of GNPs.

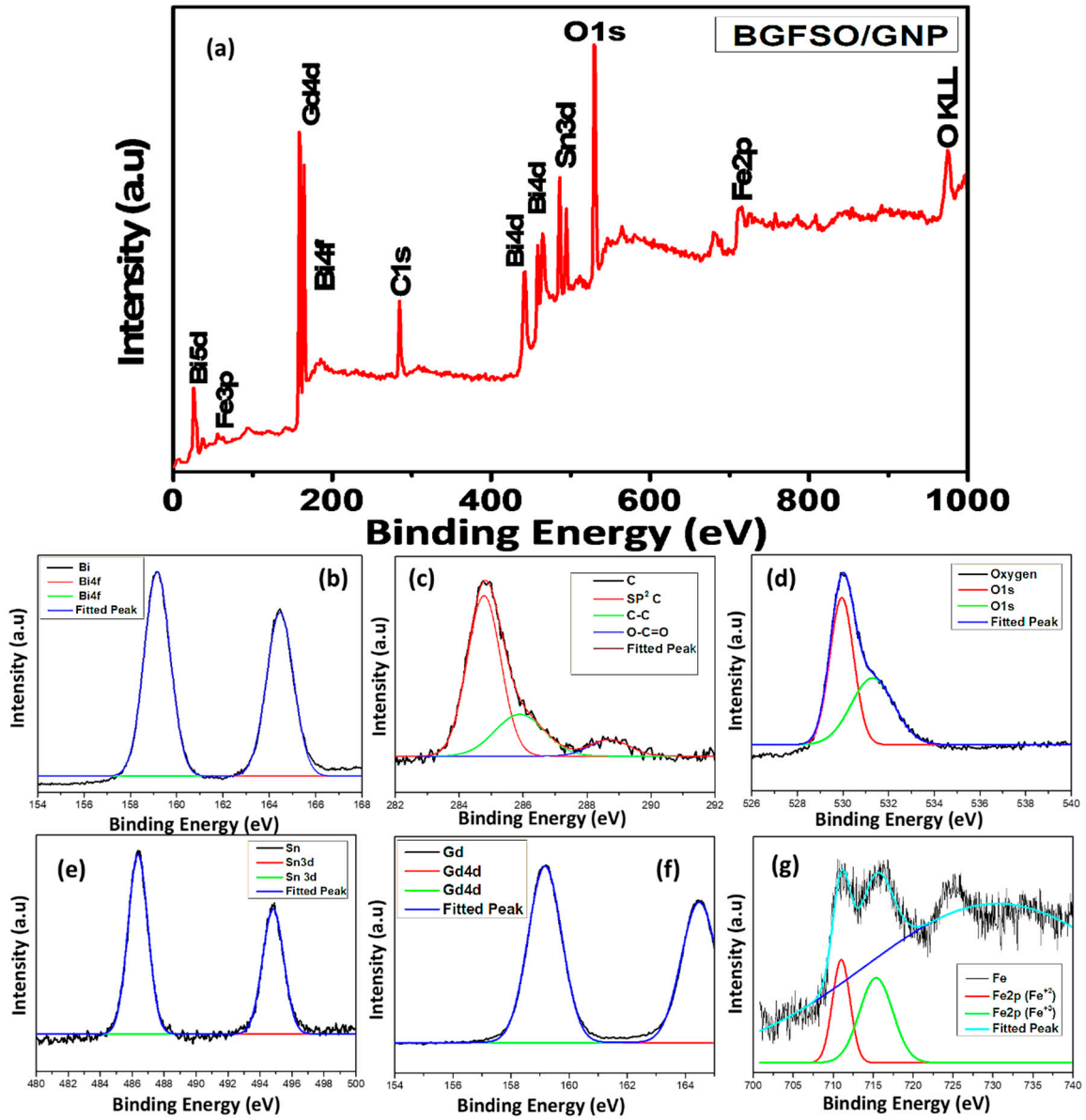

Figure 4. **(a)**. XPS analysis of BGFSO/GNP nanohybrid, **(b)** Lorentzian–Gaussian curve fitting of Bismuth (Bi), **(c)** Carbon (C), **(d)** Oxygen (O), **(e)** Tin (Sn), **(f)** Gadolinium (Gd) and **(g)** Iron (Fe).

3.3. Absorption Analysis and Band-gap Calculations

The UV-vis absorption or diffusion reflectance spectra of the BFO nanoparticles and BGFSO/GNP nanohybrids is shown in Figure 5. As BFO is a UV light active photocatalyst and has a band-gap of around 2.04 eV, it has very low absorbance of visible light. While, absorption analysis of nanohybrids demonstrates that our synthesized BGFSO/GNP has absorption in both UV and visible light ranges, as the spectra is almost linear in the whole range. The maximum absorption was obtained at wavelength 496 nm [21].

Band edge absorption was checked using kubelka Munk function [51] exhibiting,

$$(\alpha h\upsilon)^2 = A(h\upsilon - Eg)^n.$$

Here, A represents a constant while Eg, υ and h corresponds band energy, light frequency and Planck's constant. The tauc's plot representing the curves for band-gap measurements is shown in Figure 6. The band-gap calculations showed that the band-gap values are in the range of 1.91 eV

to 2.1 eV which represents that there is only a slight variation inside the band-gap of nanohybrids, as compared to pure BFO. The variation in band-gap depends on different parameters, including dopant concentration, alteration in crystallite size and lattice parameters and the materials' morphology [52]. So the optical band-gap of our system is not much effected by all these factors. The hence prepared BGFSO/GNP nanohybrids will work actively in the whole range of ultraviolet and visible light. They are the catalyst which will perform an enhanced catalytic activity by absorbing both UV and visible light as compared to BFO.

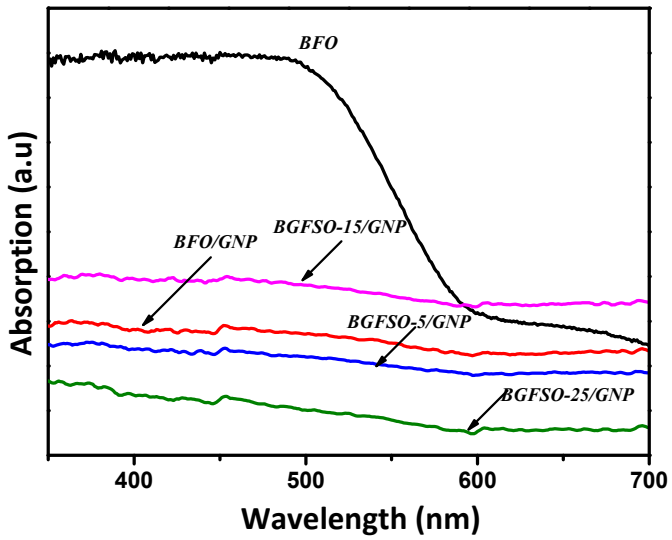

Figure 5. UV-vis absorption spectra (DRS spectra) of BFO, BFO/GNP and BGFSO/GNP nanohybrids.

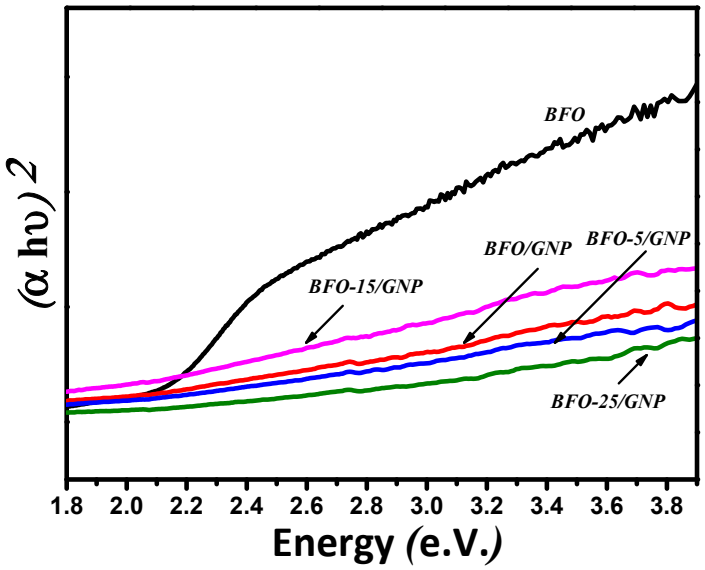

Figure 6. The tauc's plot of BGFSO/GNP nanohybrids representing curves for band-gap measurement.

3.4. Photocatalytic Activity of Nanohybrids

As prepared BGFSO-GNP nanohybrids were further subjected to photocatalytic measurements for checking their efficiency in degrading organic dye Congo-red (CR). The photocatalytic activities of BGFSO/GNP nanohybrids are shown in Figure 7, indicating that the synthesized nanohybrids provide fast removal of organic dye compared with pure BFO, due to the presence of both BGFSO and GNP phases inside nanohybrids. The nanohybrids demonstrate dye removal ability under both dark (in the absence of light) as well as visible light. The dye removal efficiencies under dark and light are referred

as catalytic activities and photocatalytic activities of nanohybrids. The catalytic activity of BFO/GNP, BGFSO-5/GNP, BGFSO-15/GNP, BGFSO-20/GNP and BGFSO-25/GNP is 32%, 48%, 44%, 56% and 51% which is due to dye adsorption on the hybrid surface under dark conditions. The photocatalytic activity of BFO/GNP, BGFSO-5/GNP, BGFSO-15/GNP, BGFSO20/GNP and BGFSO-25/GNP is 30%, 12%, 15%, 3% and 23%, respectively. The overall degradation efficiency of pure BFO is 44% in 120 min while the degradation efficiency for BFO/GNP is 62%, BGFSO-5/GNP is 60%, BGFSO-15/GNP is 59%, BGFSO-20/GNP is 59% and BGFSO-25/GNP is 74%, respectively. An already published work [23] showed a good CR dye removal with BGFSO-5 nanoparticles under visible light, but there was no dye removal under dark conditions. This demonstrates that catalysts become active in both light and dark, and are more favorable towards catalytic applications than already published work, due to incorporation of GNPs inside nanoparticles [23,31]. In addition, GNPs provide dye to adsorb over BGFSO/GNP nanohybrids surface actively, which further helped in the fast organic dye removal even in the absence of visible light [14].

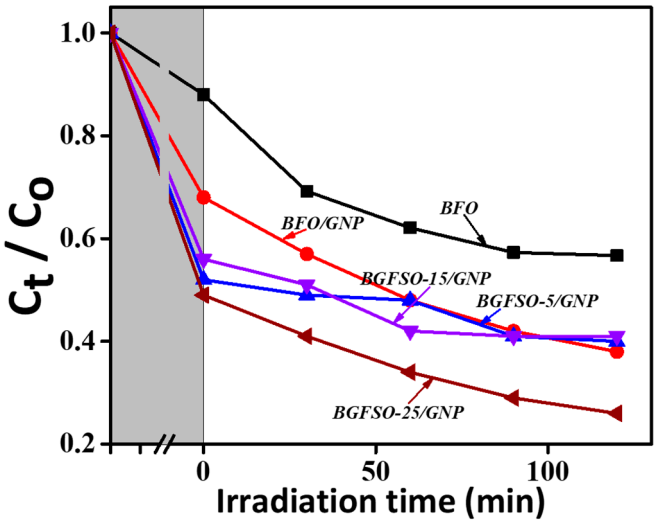

Figure 7. Photocatalytic activities of BFO particles, BFO/GNP and BGFSO/GNP nanohybrids.

In Figure 8, the catalytic activities versus Sn concentrations graph of BFO/GNP, BGFSO-5/GNP, BGFSO-15/GNP, BGFSO-20/GNP and BGFSO-25/GNP, under both light and dark, is shown in comparison wtih pure BFO. The black color inside the graph represents catalysis under dark, while the red color inside the graph represents photocatalysis under visible light. The % values of the catalytic activities of all the nanohybrids are also separately provided in the Table 1. All the nanohybrids actively worked under dark and played an efficient role in dye removal due to presence of free electrons and oxygen containing species [43,44] inside graphene sheets originated during fabrication of GNPs. In addition, they also worked under visible light for dye removal. The most active catalyst under dark is BGFSO-20/GNP and the most active photo-catalyst under visible light is BGFSO-25/GNP.

Table 1. The % dye-removal of the nanohybrid catalysts under both, light and dark conditions.

Catalyst	Dye Removal Under Dark	Dye Removal Under Light	Total Catalytic Activity
BFO/GNP	32%	30%	62%
BGFSO-5/GNP	48%	12%	60%
BGFSO-15/GNP	44%	15%	59%
BGFSO-20/GNP	56%	3%	59%
BGFSO-25/GNP	51%	23%	74%

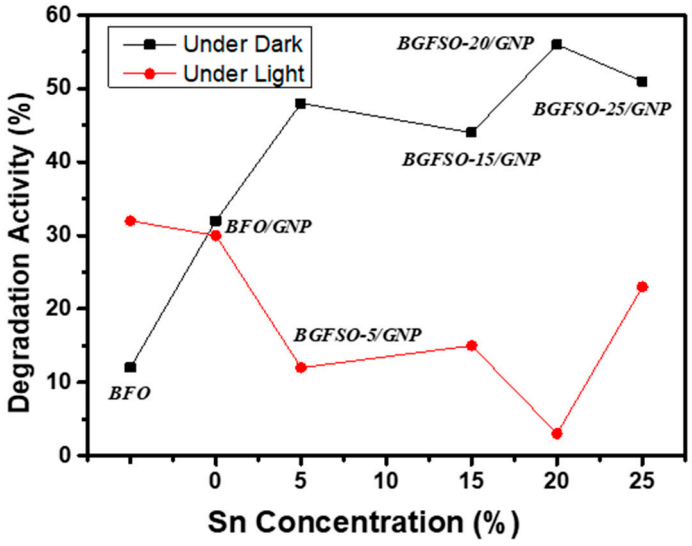

Figure 8. The dye degradation activity (%) vs. Sn concentration (%) inside BGFSO/GNP nanohybrids.

4. Dye Degradation Mechanism

The overall catalysis of organic dye depends on dye degradation in the absence and presence of visible light. Figure 9 illustrates the basic mechanism of dye degradation under visible light, as well as in the dark (absence of light).

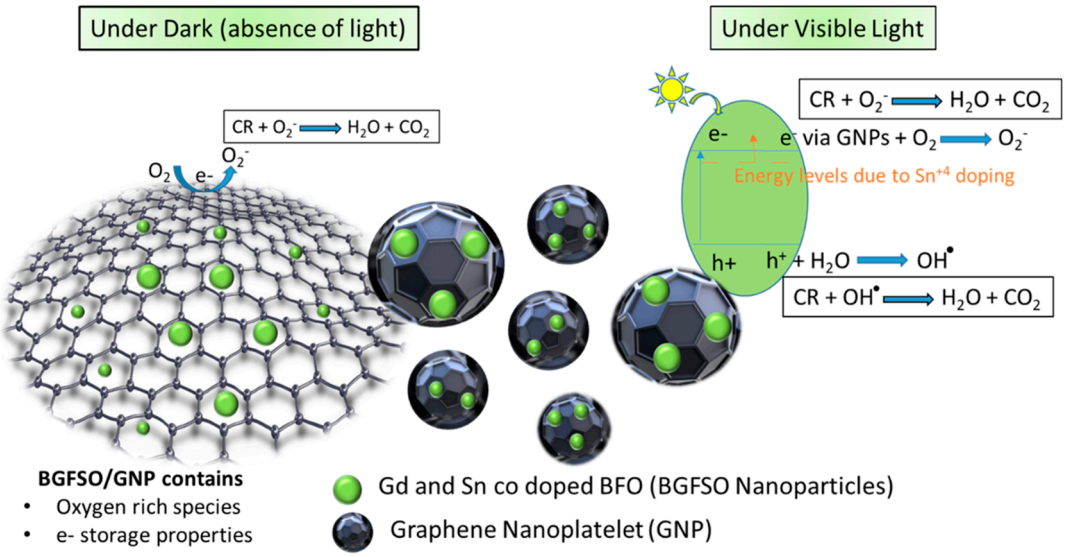

Figure 9. The catalytic mechanism inside BGFSO/GNP nanohybrids under both dark and visible light.

In the presence of light, electrons travels to the conduction band of BGFSO nanoparticles, from the valence band and the donor shallow energy levels, created below the bottom of conduction band due to the doping of Sn [10]. GNPs lower the recombination rate of electron-hole charge carriers by acting as trapping site of electron [14]. These electrons (e^-) capture oxygen (O_2) from the environment produce superoxide radicals (O_2^-), and further react with the CR dye molecules and form water (H_2O) and carbon dioxide (CO_2) as degradation by products. The water molecule on absorbing the hole (h^+) gives $OH^{\cdot}$ radicals which on further reactions produce H_2O and CO_2 as by products. The basic steps in equate form are as follows:

$$\text{BGFSO/GNP} + \text{Visible Light} \rightarrow \text{Electron Generation } (e^-)$$

$$e^{-}(BGFSO)+O_2 \rightarrow O_2^{-}$$

$$e^{-}(GNPs)+O_2 \rightarrow O_2^{-}$$

$$h^{+}+H_2O \rightarrow OH^{\bullet}$$

$$CR + O_2^{-} \rightarrow H_2O + CO_2$$

$$CR + OH^{\bullet} \rightarrow H_2O + CO_2$$

BGFSO/GNP nanohybrids as a whole contains both oxygen rich species (hydroxyl and oxy ions) as well as trapping sites of electrons [14,44]. The graphene sheets inside the GNPs has the ability to store the electrons inside the π−π carbon network during the reduction process [53]. The oxygen containing species, with the stored electrons, help scavenge the reactive catalytic carriers (e^{-}) and holes (h^{+}), even in the absence of light, thereby further initiating the degradation phenomenon by reacting with organic dye. On the other hand, graphene facilitates quicker adsorption of organic dye due to its large surface area and due to the electrostatic interaction between the dye and graphene surface [14,16]. Therefore, nanohybrids maximum degradation occurs under dark conditions due to the high adsorption and presence of reactive carriers (e^{-} h^{+}) inside the BGFSO/GNP. The catalytic congo-red degradation phenomenon has been observed before and published inside the GNP based system as well as MXene (both belonging to 2D materials family) with co-doped BFO [14,16,44]. The reported results showed the fast CR dye degradation under both light and dark conditions.

5. Materials and Methods

Bismuth nitrate (99% pure), Gadolinium nitrate (99% pure), Iron nitrate (98% pure), Tin powder, Ethylene glycol (≥99%), Acetic acid (≥99.5%), Graphene Nanoplatelets (GNP) (A-12, Graphene Supermarket) and Congo red were used as received.

5.1. Preparation of BGFSO Nanoparticles

BGFSO nanoparticles were synthesized by using sol-gel method [23]. The amount of Gd and Sn was introduced inside the base system BFO (ABO_3 system) using the general formula $A_xGd_{1-x}B_ySn_{1-y}O_3$. The amount of Gadolinium (Gd) was fixed (10%) and Tin (Sn) amount was varied (5% to 25%) using basic calculations for $Bi_{0.90}Gd_{0.10}Fe_{0.95}Sn_{0.05}O_3$, $Bi_{0.90}Gd_{0.10}Fe_{0.90}Sn_{0.10}O_3$, $Bi_{0.90}Gd_{0.10}Fe_{0.85}Sn_{0.15}O_3$, $Bi_{0.90}Gd_{0.10}Fe_{0.80}Sn_{0.20}O_3$, $Bi_{0.90}Gd_{0.10}Fe_{0.75}Sn_{0.25}O_3$ and as synthesized samples were named as BGFSO-5 (5% Sn), BGFSO-15 (15% Sn), BGFSO-20 (20% Sn) and BGFSO-25 (25% Sn).

5.2. Preparation of BGFSO-GNP Nanohybrids

Graphene nanoplatelets (GNPs) were dispersed in deionized (DI) water in an amount of 1 mg/mL using a bath sonicator. The BGFSO nanoparticles (0.01M) were dissolved in ethylene glycol and acetic acid (volume ratio 1:1) via sonication at 60 °C for 2 h. The GNP dispersion (1 mg/mL) and BGFSO solution were combined at room temperature and sonicated for about 15 min, followed by 60 min magnetic stirring at 85 °C. The nanohybrids settled as precipitates. The precipitates were washed three to four times with DI water, followed by vacuum filtration using Whatman 0.2 m filter paper. The filter cake was air dried for 12 h at 50°C in a convection oven. The dried samples were named BGFSO-GNP nanohybrids.

6. Conclusion

In this study BFO, BGFSO nanoparticles have been prepared using sol-gel method and BGFSO/GNP nanohybrids have been fabricated through co-precipitation method and then further characterizations. XRD, SEM and TEM were carried out for structural and morphological analysis, which shows a smooth dispersion of spherical BGFSO particles over GNP sheets. Absorption analysis showed that nanohybrids

absorb both UV and visible light, and act the same under both ranges. The photocatalytic application further represented that catalyst are active, not even under visible light, but also in dark conditions and proved to be more efficient catalytic material for organic dye removal during water purification. The free electrons and oxygen species inside graphene sheets played a role in oxidation/reduction reactions and helped in degradation of organic dye. The easy synthesized nanohybrids, with enhanced dye removal, proved to be more encouraging for photocatalytic applications.

Author Contributions: S.F. and S.I.A. equally contributed to the manuscript; performed the material synthesis, characterizations and data analysis with manuscript writing, M.Z.I. helped extensively in paper writing, data analysis and S.R. designed and supervised the whole project. All authors have read and agreed to the published version of the manuscript.

Funding: This research was funded by Higher Education Commission (HEC) of Pakistan under the project no. 6040/Federal/NRPU/R&D/HEC/2016, HEC/USAID under the project no. HEC/R&D/PAKUS/2017/783, Emirates Center for Energy and Environment Research through grant # 31R166.

Acknowledgments: The authors are thankful to the Higher Education Commission (HEC) of Pakistan for providing research funding under the project no. 6040/Federal/NRPU/R&D/HEC/2016 and HEC/USAID and financial support under the project no. HEC/R&D/PAKUS/2017/783. The author is grateful to the School of Natural Sciences (SNS) at the National University of Science & Technology (NUST), Islamabad, Pakistan, for partial financial support. Partial financial support for this project was provided from Emirates Center for Energy and Environment Research through grant # 31R166.

Conflicts of Interest: The authors declare no conflict of interest.

References

1. Fujishima, A.; Zhang, X.; Tryk, D.A. TiO_2 photocatalysis and related surface phenomena. *J. Adv. Mater.* **2018**, *63*, 515–582. [CrossRef]
2. Rife, R.; Thomas, T.W.; Norberg, D.W.; Fournier, R.L.; Rinker, F.G.; Bonomoi, M.S. Chemical Demilitarization: Disposing of the Most Hazardous Wastes. *Environ. Prog.* **1989**, *8*, 167–175. [CrossRef]
3. Xu, N.; Shi, Z.; Fan, Y.; Dong, J.; Shi, J.; Hu, M.Z.C. Effects of Particle Size of TiO_2 on Photocatalytic Degradation of Methylene Blue in Aqueous Suspensions. *Chem. Rev.* **1999**, *38*, 373–379.
4. Henderson, M.A. A surface science perspective on TiO_2 photocatalysis. *Surf. Sci. Rep.* **2011**, *66*, 185–297. [CrossRef]
5. Tada, H.; Hattori, A.; Tokihisa, Y.; Imai, K.; Tohge, N.; Ito, S. A Patterned-TiO_2/SnO_2 Bilayer Type Photocatalyst. *J. Phys. Chem. B* **2000**, *104*, 4585–4587. [CrossRef]
6. Hoffmann, M.R.; Martin, S.T.; Choi, W.; Bahnemann, D.W. Environmental Applications of Semiconductor Photocatalysis. *Chem. Rev.* **1995**, *95*, 69–96. [CrossRef]
7. Tan, Z.K.; Moghaddam, R.S.; Lai, M.L.; Docampo, P.; Highler, R.; Deschler, F.; Price, M.; Sadhanala, A.; Pazos, L.M.; Credgington, D.; et al. Bright light-emitting diodes based on organometal halide perovskite. *Nat. Nanotechnol.* **2014**, *9*, 687–692. [CrossRef]
8. Hu, G.D.; Cheng, X.; Wu, W.B.; Yang, C.H. Effects of Gd substitution on structure and ferroelectric properties of $BiFeO_3$ thin films prepared using metal organic decomposition. *Appl. Phys. Lett.* **2007**, *91*, 1–3. [CrossRef]
9. Green, M.A.; Ho-Baillie, A.; Snaith, H.J. The emergence of perovskite solar cells. *Nat. Photon* **2014**, *8*, 506–514. [CrossRef]
10. Sobhan, M.; Xu, Q.; Zhao, J.; Franklin, A.; Hu, Y.; Tse, J.S.; Wu, P. Modification of surface chemistry by lattice Sn dopingin $BiFeO_3$ nanofibers. *Europhys. Lett.* **2015**, *111*, 1–5. [CrossRef]
11. Schmid, H. Multi-ferroic magnetoelectrics. *Ferroelectrics* **1994**, *162*, 317–338. [CrossRef]
12. Kube, F.; Schmid, H. Structure of a ferroelectric and ferroelastic monodomain crystal of the perovskite $BiFeO_3$. *Acta Crystallogr.* **1990**, *B46*, 698–702. [CrossRef]
13. Yin, J.; Zou, Z.; Yee, J. Photophysical and Photocatalytic Activities of a Novel Photocatalyst $BaZn_{1/3}Nb_{2/3}O_3$. *J. Phys. Chem. B* **2004**, *108*, 12790–12794. [CrossRef]
14. Fatima, S.; Ali, S.I.; Iqbal, M.Z.; Rizwan, S. Facile The high photocatalytic activity and reduced band gap energy of La and Mn co-doped $BiFeO_3$/graphene nanoplatelet (GNP) nanohybrids. *RSC Adv.* **2017**, *7*, 35928–35937. [CrossRef]

15. Kanhere, P.; Chen, Z. A Review on Visible Light Active Perovskite-Based Photocatalysts. *Molecules* **2014**, *19*, 19995–20022. [CrossRef] [PubMed]
16. Fatima, S.; Ali, S.I.; Younas, D.; Islam, A. Graphene nanohybrids for enhanced catalytic activity and large surface area. *MRS Comm.* **2018**, *1*, 27–36. [CrossRef]
17. Tariq, A.; Irfan, S.; Akinwande, D.; Rizwan, S. Efficient Visible-Light Photocatalysis of 2D-MXene Nanohybrids with Gd^{3+}- and Sn^{4+} -Codoped Bismuth Ferrite. *ACS Omega* **2018**, *3*, 13828–13836. [CrossRef]
18. Umer, M.; Mahmood, N.; Awan, S.U.; Fatima, S.; Mahmood, A.; Rizwan, S. Rationally designed La and Se co-doped bismuth ferrites with controlled bandgap for visible light photocatalysis. *RSC Adv.* **2019**, *30*, 17148–17156. [CrossRef]
19. Irfan, S.; Rizwan, S.; Shen, Y.; Tomovska, R.; Zulfiqar, S.; Sarwar, M.I.; Nan, C.W. Mesoporous template-free gyroid-like nanostructures based on La and Mn co-doped Bismuth ferrites with improved photocatalytic Activity. *RSC Adv.* **2016**, *6*, 114183–114189. [CrossRef]
20. Wang, S.; Chen, D.; Niu, F.; Zhang, N.; Qin, L.; Huang, Y. Pd cocatalyst on Sm-doped $BiFeO_3$ nanoparticles: Synergetic effect of a Pd co-catalyst and samarium doping on photocatalysis. *RSC Adv.* **2016**, *6*, 34574–34587. [CrossRef]
21. Zhang, N.; Chen, D.; Niu, F.; Wang, S.; Qin, L.; Huang, Y. Enhanced visible light photocatalytic activity of Gd-doped $BiFeO_3$ nanoparticles and mechanism insight. *Sci. Rep.* **2016**, *6*, 26467. [CrossRef] [PubMed]
22. Guo, R.; Fang, L.; Dong, W.; Zheng, F.; Shen, M. Enhanced Photocatalytic Activity and Ferromagnetism in Gd Doped $BiFeO_3$ Nanoparticles. *J. Phys. Chem. C* **2010**, *114*, 21390–21396. [CrossRef]
23. Irfan, S.; Rizwan, S.; Shen, Y.; Li, L.; Asfandiyar; Butt, S.; Nan, C.W. The Gadolinium (Gd^{3+}) and Tin (Sn^{4+}) Co-doped $BiFeO_3$ Nanoparticles as New Solar Light Active Photocatalys. *Sci. Rep.* **2017**, *7*, 42493. [CrossRef] [PubMed]
24. Li, Z.; Shen, Y.; Yang, C.; Lei, Y.; Guan, Y.; Lin, Y.; Liu, D.; Nan, C.W. Significant enhancement in the visible light photocatalytic properties of $BiFeO_3$-graphene nanohybrids. *J. Mater. Chem. A* **2012**, *1*, 823–829. [CrossRef]
25. Li, T.; Shen, J.; Li, N.; Ye, M. Hydrothermal preparation, characterization and enhanced properties of reduced graphene-$BiFeO_3$ nanocomposite. *Mater. Lett.* **2013**, *91*, 42–44. [CrossRef]
26. Sun, A.; Chen, H.; Song, C.; Jiang, F.; Wang, X.; Fu, Y. Magnetic $Bi_{25}FeO_{40}$-graphene catalyst and its high visible-light photocatalytic performance. *RSC Adv.* **2013**, *3*, 4332–4340. [CrossRef]
27. Soltani, T.; Lee, B.K. Sono-synthesis of nanocrystallized $BiFeO_3$/reduced graphene oxide composites for visible photocatalytic degradation improvement of bisphenol A. *Chem. Eng. J.* **2016**, *306*, 204–213. [CrossRef]
28. Reetu; Agarwal, A.; Sanghi, S.; Hooda, A. Rietveld analysis, dielectric and magnetic properties of Sr and Ti codoped $BiFeO_3$ multiferroic. *J. Appl. Phys.* **2016**, *110*, 073909–073915.
29. Yin, L.H.; Song, W.H.; Jiao, X.L.; Wu, W.B.; Zhu, X.B.; Yang, Z.R.; Dai, J.M.; Zhang, R.L.; Sun, Y.P. Multiferroic and magnetoelectric properties of Bi1−xBaxFe1−xMnxO_3 system. *J. Phys. D Appl. Phys.* **2009**, *42*, 205402–205407. [CrossRef]
30. Do, D.; Kim, J.W.; Kim, S.S. Effects of Dy and Mn co doping ferroelectric properties of $BiFeO_3$ thin films. *J. Am. Ceram. Soc.* **2011**, *94*, 2792–2797. [CrossRef]
31. KianI, M.; Kiani, A.B.; Khan, S.Z.; Rehmana, S.; Khan, Q.U.; Mahmood, I.; Saleemi, A.S.; Jalil, A.; Sohail, M.; Zhu, L. Facile synthesis of Gd and Sn co-doped $BiFeO_3$ supported on nitrogen doped graphene for enhanced photocatalytic activity. *J. Phys. Chem. Solids* **2019**, *130*, 222–229. [CrossRef]
32. Akhavan, O. Graphene Nanomesh by ZnO Nanorod Photocatalysts. *ACS Nano* **2010**, *4*, 4174–4180. [CrossRef] [PubMed]
33. Novoselov, K.S.; Geim, A.K.; Morozov, S.V.; Jiang, D.; Katsnelson, M.I.; Grigorieva, I.V.; Dubonos, S.V.; Firsov, A.A. Two Dimensional Gas of Massless Dirac Fermions in Graphene. *Nature* **2005**, *438*, 197–200. [CrossRef] [PubMed]
34. Sakamoto, J.; Heijst, J.V.; Lukin, O.; Schluter, A.D. TwoDimensional Polymers: Just a Dream of Synthetic Chemists. *Angew. Chem. Int. Ed.* **2009**, *48*, 1030–1069. [CrossRef]
35. Doustkhah, E.; Ide, Y. Microporous layered silicates: Old but new microporous materials. *New J. Chem.* **2020**, in press. [CrossRef]
36. Xu, C.; Wang, X.; Zhu, J. Graphene-Metal Particle Nanocomposites. *J. Phys. Chem. C* **2008**, *112*, 19841–19845. [CrossRef]

37. Rostamnia, S.; Doustkhah, E.; Karimi, Z.; Amini, S.; Luque, R. Surfactant-Exfoliated Highly Dispersive Pd-Supported Graphene Oxide Nanocomposite as a Catalyst for Aerobic Aqueous Oxidations of Alcohols. *ChemCatChem* **2015**, *7*, 1678–1683. [CrossRef]
38. An, J.; Zhu, L.; Wang, N.; Song, Z.; Yang, Z.; Du, D.; Tang, H. Photo-Fenton like degradation of tetrabromobisphenol A with graphene $BiFeO_3$ composite as a catalyst. *Chem. Eng. J.* **2013**, *219*, 225–237. [CrossRef]
39. Nieto, A.; Lahiri, D.; Agarwal, A. Synthesis and properties of bulk graphene nanoplatelets consolidated by spark plasma sintering. *Carbon* **2012**, *50*, 4068–4077. [CrossRef]
40. Kavan, L.; Yum, J.H.; Grtzell, M. Optically Transparent Cathode for Dye-Sensitized Solar Cells Based on Graphene Nanoplatelets. *ACS Nano* **2010**, *5*, 165–172. [CrossRef]
41. Han, J.; Zhang, L.L.; Lee, S.; Oh, J.; Lee, K.S.; Potts, J.R.; Ji, J.; Zhao, X.; Ruoff, R.S.; Park, S. Generation of B-Doped Graphene Nanoplatelets Using a Solution Process and Their Supercapacitor Applications. *ACS Nano* **2012**, *7*, 19–26. [CrossRef] [PubMed]
42. Arshad, A.; Iqbal, J.; Siddiq, M.; Mansoor, Q.; Ismail, M.; Mehmood, F.; Ajmal, M.; Abid, Z. Graphene nanoplatelets induced tailoring in photocatalytic activity and antibacterial characteristics of MgO/graphene nanoplatelets nanocomposites. *ACS Omega* **2019**, *4*, 8661–8668. [CrossRef]
43. Lakshmi, V.; Rajagopalan, V. A New Synergetic Nanocomposite for Dye Degradation in Dark and Light. *Sci. Rep.* **2016**, *6*, 38606.
44. Iqbal, M.A.; Irfan, S.; Amin, F.; Tariq, A.; Iqbal, M.Z.; Rizwan, S. La- and Mn-Codoped Bismuth Ferrite/Ti3C2 MXene Composites for Efficient Photocatalytic Degradation of Congo Red Dye. *ACS Omega* **2018**, *4*, 4053–4062. [CrossRef] [PubMed]
45. Guerra, V.; Wan, C.; Degirmenci, V.; Solan, J.; Presvytis, D.; Watson, M.; McNally, T. Characterisation of graphite nanoplatelets (GNP) prepared at scale by high-pressure homogenisation. *J. Mater. Chem. C* **2019**, *7*, 6383–6390. [CrossRef]
46. Batakliev, T.; Doycheva, I.P.; Angelov, V.; Georgiev, V.; Ivanov, E.; Kotsilkova, R.; Casa, M.; Cirillo, C.; Adami, R.; Sarno, M.; et al. Effects of Graphene Nanoplatelets and Multiwall Carbon Nanotubes on the Structure and Mechanical Properties of Poly(lactic acid) Composites: A Comparative Study. *Appl. Sci.* **2019**, *9*, 469. [CrossRef]
47. Das, R.; Sarkar, T.; Mandal, K. Multiferroic properties of Ba^{2+} and Gd^{3+} co-doped bismuth ferrite: Magnetic, ferroelectric and impedance spectroscopic analysis. *J. Phys. D Appl. Phys.* **2012**, *45*, 455002. [CrossRef]
48. Wang, F.; Drzal, L.T.; Qin, Y.; Huang, Z. Effects of functionalized graphene nanoplatelets on the morphology and properties of epoxy resins. *High Perform. Polym.* **2015**, *28*, 525–536. [CrossRef]
49. Johra, F.T.; Lee, J.W.; Jung, W.G. Facile and safe graphene preparation on solution based platform. *J. Ind. Eng. Chem.* **2014**, *20*, 2882–2887. [CrossRef]
50. Sun, R.; Yao, H.; Zhang, H.B.; Li, Y.; Mai, Y.W.; Yu, Z.Z. Decoration of defect-free graphene nanoplatelets with alumina for thermally conductive and electrically insulating epoxy composites. *Compos. Sci. Technol.* **2016**, *137*, 16–23. [CrossRef]
51. Kubelka, P.; Munk, F. Ein Beitrag Zur Optik Der Farbanstriche. *Tech. Phys.* **1931**, *12*, 593–601.
52. Irfan, S.; Liang, G.X.; Li, F.; Chen, Y.X.; Rizwan, S.; Jin, J.; Zhuanghao, Z.; Ping, F. Effect of Graphene Oxide Nano-Sheets on Structural, Morphological and Photocatalytic Activity of $BiFeO_3$-Based Nanostructures. *Nanomaterials* **2019**, *9*, 1337. [CrossRef] [PubMed]
53. Lightcap, I.V.; Kosel, T.H.; Kamat, P.V. Anchoring Semiconductor and Metal Nanoparticles on a 2-Dimensional Catalyst Mat. Storing and Shuttling Electrons with Reduced Graphene Oxide. *Nano Lett.* **2010**, *10*, 577–583. [CrossRef] [PubMed]